Astron. Astrophys. 352, 645–658 (1999)

ASTRONOMY AND ASTROPHYSICS

Optical images of MCLD123.5+24.9: a cloud illuminated by the North star?

F. Zagury[1,2], **F. Boulanger**[2], **and V. Banchet**[3]

[1] Department of Astrophysics, Nagoya University, Nagoya, 464-01 Japan (zagury@a.phys.nagoya-u.ac.jp)
[2] Institut d'Astrophysique Spatiale, Université Paris Sud, Bat. 121, 91405 Orsay Cedex, France
[3] Institut d'Astrophysique de Paris, 65 Bd. Arago, 75005 Paris, France

Received 15 July 1999 / Accepted 22 September 1999

Abstract. We present B R I images of a $1^\circ \times 1^\circ$ field centered on the molecular cloud (MCLD123.5+24.9) located in the large infrared cirrus known as the Polaris Flare. The optical images are compared with IRAS images and an extinction map derived from stellar reddenings. We analyse the possibility for the North star (HD8890), only 1° North of the field, to be the source of MCLD123.5+24.9 optical emission. For widely accepted values of the dust albedo ($\omega = 0.6$) and the assymetry parameter of the Henyey Greenstein phase function ($0.7 < g_0$), forward scattering of Polaris light explains the cloud optical brightness, colors, and the surface brightness ratios derived from comparison of optical and $100\,\mu$m data. The cloud colors are redder than what is expected from diffusion of Polaris light by a low column density medium, but the color difference may be explained by extinction with no need for red luminescence. Within this interpretation, the cloud is located between 105 and 125 pc from the Sun and is 6 to 25 pc in front of Polaris. Over this range of distances, due to forward scattering, Polaris is the main source of the cloud optical emission but a minor source of dust heating relative to the general Galactic interstellar radiation field of the Solar neighborhood (ISRF).

Key words: ISM: clouds – ISM: dust, extinction – ISM: individual objects: MCLD123.5+24.9 – stars: individual: Polaris = HD 8890 – scattering

1. Introduction

Images of nearby clouds in the optical bands often provide a spectacular view at the small scale structure of the interstellar medium. The high resolution achieved at optical wavelengths is of obvious interest for the study of interstellar clouds structure: the 2" pixel size corresponds to a spatial resolution of $10^{-3}\,\mathrm{pc} = 200\,\mathrm{A.U.}$ for a cloud at $100\,\mathrm{pc}$ to the Sun. Interpretation of optical emission will rely on the identification of the radiation field and knowledge of grain properties.

The source of light can be either a specific star or the general Galactic interstellar radiation field (ISRF). Since the early work of Henyey & Greenstein (1941) on the diffuse Galactic light and that of Mattila (1971) on dark nebulae, diffuse optical emission of high galactic latitude clouds (HLCs) has been studied with the assumption that ISRF is the illuminating source.

Interstellar dust grains have a screen-like effect on photons and optical emission of nebulae at wavelength λ is usually interpreted as light scattered by interstellar grains of size $\sim \lambda/(2\pi)$ and larger. Considering the size distribution of interstellar dust particles, this places them amongst the largest grains which also produce the far-infrared (thermal) emission of the interstellar medium. Similarity and proportionality are thus expected between optical images and IRAS $100\,\mu$m image, at least for column densities which are not too high. The optical and far-infrared diffuse emission from cirrus clouds have been observed to correlate to a significant extent (de Vries & Le Poole 1985, Guhathakurta & Tyson 1989, Paley et al. 1991).

Knowledge of the radiation field and grain properties allows quantitative comparison between observed and expected optical emission of nebulae. Colors are especially useful because they do not directly depend on several parameters such as the absolute strength of the radiation field, the distance to the illuminating star and the phase function, which are difficult to evaluate. In some reflection nebulae it was found that extinction effects alone cannot explain the observed colors (Witt & Schild 1985). In addition to scattering, luminescence seems necessary to account for a broad spectroscopic bump in the R band, referred to as ERE (Extended Red Emission). Luminescence in the R and I bands has also been postulated to explain the colors and spectra of several infrared cirrus (Guhathakurta & Tyson 1989, Szomoru & Guhathakurta 1999) and the B-R color of the diffuse Galactic light (Gordon et al. 1998). Crystalline nanoparticles of pure silicon have been proposed as potential carriers of the ERE (Ledoux et al. 1998, Witt et al. 1998). However, the existence of such peculiar particles in the interstellar medium seems quite speculative. Further, to match the Gordon et al. estimate of the red lumninescence intensity per H atom with the extinction curve, it is necessary that the ERE emitting particles have an extreme luminescence photon conversion efficiency close to 100% (Zubko et al. 1999).

Line emission from different molecules in our particular field, MCLD $123.5 + 24.9$, $\sim 1^\circ$ from the North star (Polaris,

Send offprint requests to: F. Zagury

HD8890), have been presented by Großmann et al. (1990, 1992). Large column density fluctuations across the field and high density clumps ($n_H >$ a few 10^3 cm^{-3}) are reported in these 2 studies (see also Falgarone et al. 1998). The spectacular features seen in the I band image (Fig. 1) may, in part, reflect those fluctuations.

Before any quantitative analysis of the optical images of MCLD $123.5+24.9$, it is necessary to have a good understanding of the radiation field that illuminates the cloud. This is the purpose of this paper. The questions we wish to answer herein are:

- To what extent the relation between the optical and the infrared IRAS $100\,\mu$m emissions can be understood.
- Which radiation field is responsible for the diffuse optical emission of the cloud and for the infrared emission? In particular, can this radiation field account for the optical brightnesses and colors?
- Do we need red luminescence to explain MCLD $123.5+24.9$ colors?

To answer those questions we focus on the lowest column density parts of the images, where interpretation of optical colors and comparison of optical and infrared images are easiest to understand (Sect. 3). We show that MCLD 123.5+24.9 cloud might well be in front of the Polaris star (Sect. 4 and appendix A). Within this hypothesis, its optical emission can be explained by forward scattering of Polaris light (Sects. 5 and 6).

2. Observations and data reduction

2.1. Observations and image mosaicing

The images presented here come from 2 observing runs in 1995 and 1996 at the 0.6/0.9-m (corrector, primary mirror) Burrell Schmidt telescope at Kitt Peak National Observatory. A tektronix 2048×2048 CCD camera, with a scale of about $2''$/pixel was used. CCD images were obtained through standard BRI filters with many 10 minute frames slightly shifted with respect to one another, yielding an effective exposure time above 1 hr per filter.

Observations were made by Roc Cutri and Frédéric Zagury. Roc Cutri made the data reduction, flatfielding and calibration. He provided the combined images of this study. Flatfields (one per filter) are obtained by adding all the images of the different objects which were observed during the 3 days run. Standart stars were repeatedly observed to provide the images calibration. It was checked on stars with known magnitudes within the image. The calibration is believed to be good within 10%.

The noise level can reach $5\,10^{-3}\,\mathrm{MJy/sr}$. It is considerably reduced by the smoothing to IRAS resolution, as shown by the perfect superimposition of cuts in the infrared and the optical (Fig. 7). This paper being restricted to a comparison of optical and infrared emission of MCLD $123.5+24.9$, noise does not critically affect our results. The main uncertainty concerning the analysis of the paper comes from straylight (Sect. 2.2).

2.2. Straylight and stars subtraction

In the original images there is a N-S gradient pointing in the direction of the North Equatorial Pole and decreasing from North to South superimposed on the MCLD $123.5+24.9$ cloud. This gradient is mostly seen in the R band and also, to a lesser extent, in the B and I bands. It varies from one exposure to another so that – excluding the possibility that these variations arise from Polaris luminosity variations – we can attribute the gradient to straylight, most probably Polaris light scattered in the Earth's atmosphere. Its maximum magnitude in the R band is $\sim\ 2\,10^{-5}$ MJy/sr/arcsec. We chose to model the gradient in each wavelength using a smooth polynomial surface of degree 2 which was subtracted from each of the optical images.

Stars and galaxies were subtracted from each image and replaced by an interpolation. This procedure greatly facilitates the study of the diffuse emission. In particular, it allows the comparison with the lower resolution IRAS data. Stars were discriminated from galaxies in order to produce a star catalogue which was used to make an extinction image of the cirrus (Fig. 3).

In Fig. 2, B and R images are shown after the polynomial surface and the stars were subtracted. The polynomial is obviously only an approximation of the true straylight pattern. For example, to the North of the optical images a bright spot with no IRAS counterpart might well be some residual straylight. In the following, the image analysis will be limited to local variations of the emission which should not be affected by residual straylight. Locally, and especially in the East-West direction, the straylight does not vary enough to modify the results presented in the following sections.

2.3. Matching optical and IRAS images

For the present study optical B and R images were reduced in size and rotated so as to match each other, pixel by pixel, over a common field of view ($\sim 1^\circ \times 1^\circ$). They were smoothed to a resolution of $8''$ per pixel and binned to lead to the 500×500 pix^2 images shown in Fig. 2.

In this paper, following previous studies of the optical emission of cirrus (de Vries & Le Poole 1985, Guhathakurta & Tyson 1989, Paley et al. 1991) we ignore the small scale structure and compare the optical and $100\,\mu$m brightness at the IRAS resolution. For this purpose, a set of optical images smoothed from the 8" resolution to a gaussian beam of $5'$ matching the IRAS resolution was realised.

The IRAS images ($60\,\mu$m, $100\,\mu$m, from ISSA plates) were interpolated on the same $8''$ pixel grid as the visible images, providing a complete set of infrared and optical 500×500 images covering the same field of view (Fig. 2). The zero of the infrared emission at each wavelength was chosen from a region of the ISSA plates outside the cirrus. The offsets applied to the ISSA brightnesses are -0.69, 0.4 MJy/sr at 60 and $100\,\mu$m.

2.4. Extinction map

The stellar catalog was used to perform an extinction image (Fig. 3) of MCLD $123.5+24.9$. Following Thoraval et al. (1997)

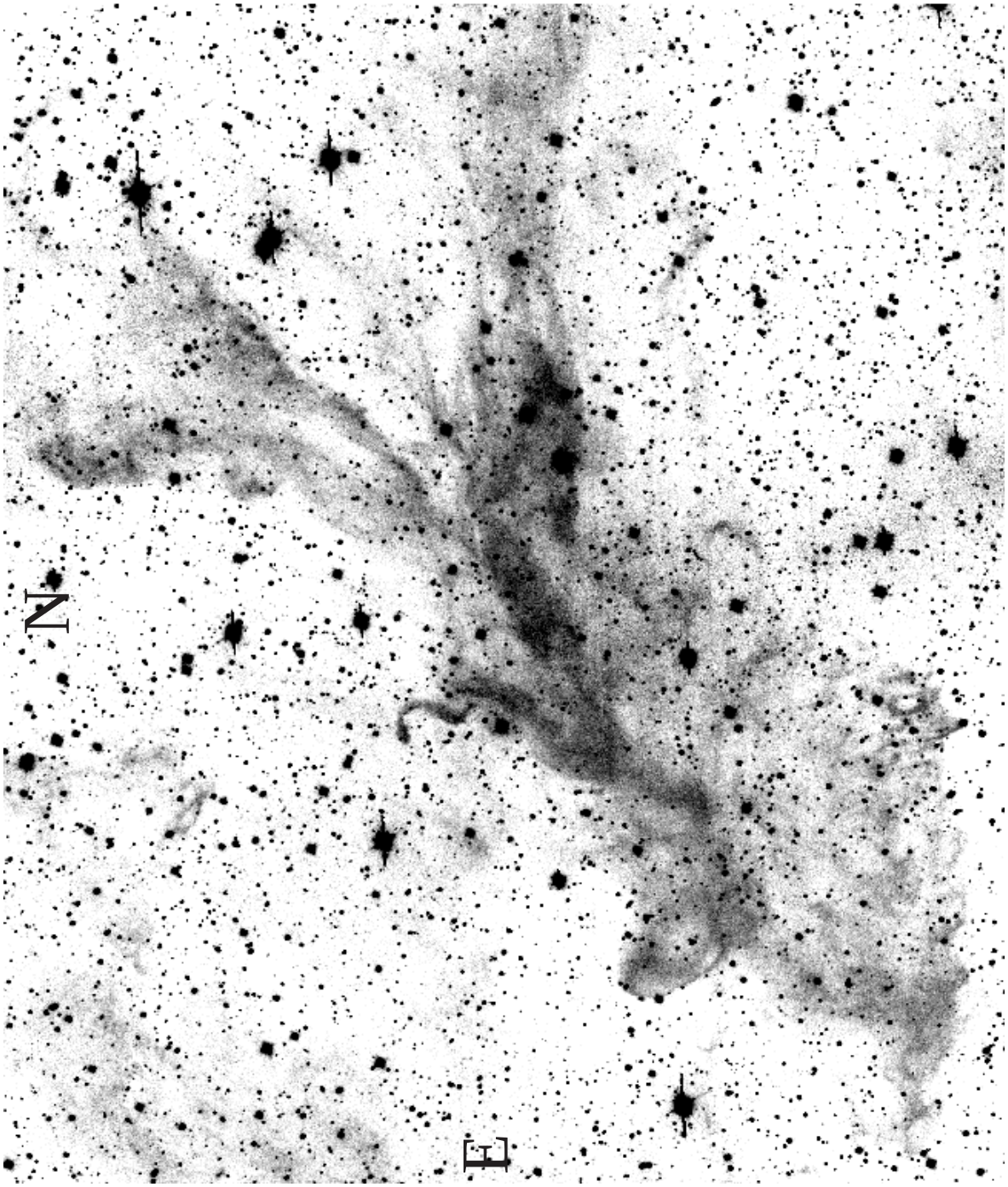

Fig. 1. I image of MCLD $123.5 + 24.9$. The field is $\sim 50' \times 43'$. It is centered on $\alpha_{1950} = 01\mathrm{h}33'$ $\delta_{1950} = 87°38'$

the extinction was estimated by taking the median value of (B-R) color of stars within $5' \times 5'$ boxes, corresponding to IRAS resolution, rather than by star counts. To measure stellar colors, we had to reduce the B and R stellar catalogs to stars detected in both B and R bands. The R band image being deeper than the B image this introduces a magnitude cut-off which is color-independent in B but decreases with B-R in R. We simulated the effect of reddening on the $(\mathrm{B} - \mathrm{R},\ \mathrm{m_R})$ color magnitude diagram starting from the colors and magnitude of the stars observed within the region of lowest extinction. This simulation shows that the true E(B-R) is 1.14 times the measured E(B-R). This scaling was applied to our data.

3. Image analysis

3.1. Infrared emission

Fig. 3 is a grey scale map of E(B-R) overlaid by $100\,\mu$m contours. The good correlation between variations in extinction and

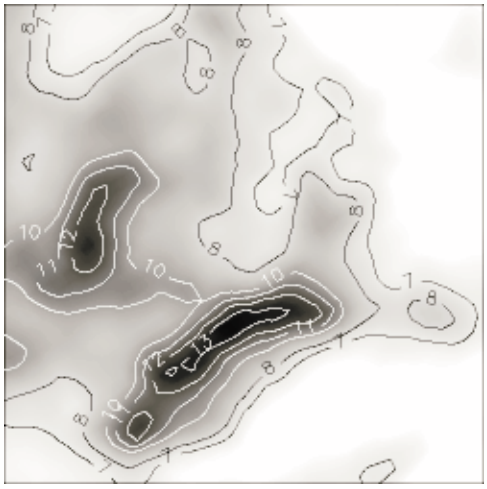

100 μm IRAS IMAGE
contours=[7, 8, 10, 12, 13] MJy/sr

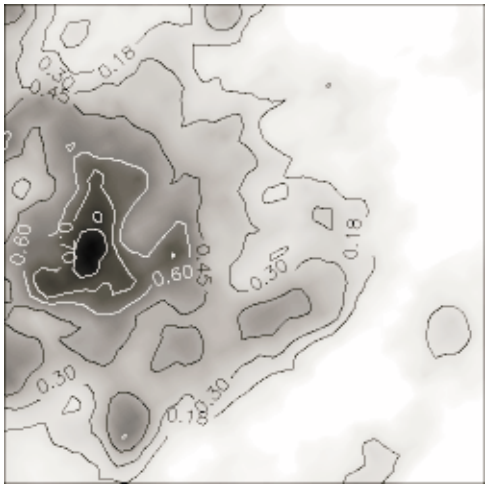

60 μm IRAS IMAGE
contours=[0.18, 0.3, 0.45, 0.6, 0.7] MJy/sr

R IMAGE

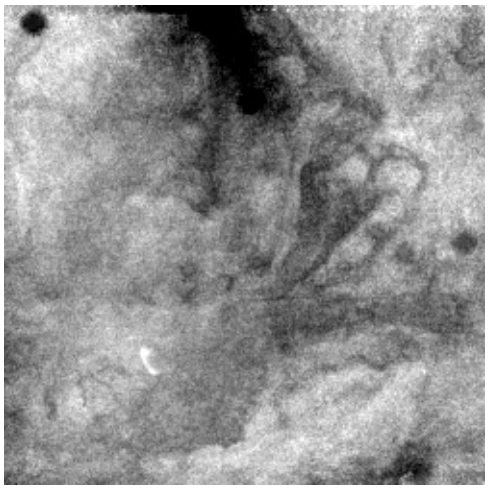

B IMAGE

Fig. 2. IRAS and optical images. IRAS and optical images are set to a common scale of 8" per pixel. The images are $500 \times 500\,\mathrm{pix}^2$ ($1^\circ \times 1^\circ$) large. Stars and galaxies have been substracted to the optical images. After substraction of the background, the optical emission varies from 0 to $\sim 0.015\,\mathrm{MJy/sr}$ for the B band and $\sim 0.032\,\mathrm{MJy/sr}$ for the R band. The round spot on the upper left corner of the B and R images corresponds to residual emission from a bright star. The dense clump mapped by Falgarone et al. (1998) is the white feature recognizable on the B image, South-East to the center of the field.

in $100\,\mu$m surface brightness is illustrated by a point to point comparison in Fig. 4. This diagram can also be used to quantify the linearly spaced grey levels of Fig. 3. E(B-R) color excess was converted to $\mathrm{A_V}$ assuming $\mathrm{R_V} = 3.1$ and $\mathrm{A_V} = 1.7\,\mathrm{E(B-R)}$ (Cardelli et al. 1989).

An important step in the comprehension of MCLD $123.5 + 24.9$ low density medium colors is the determination of the total extinction through the cloud lowest density regions. To estimate the cloud extinction in regions of low $\mathrm{I}_\nu(100\,\mu\mathrm{m})$, we compared the observed B-R stellar colors histogram to the one predicted by the Besançon Galactic model (Bienaymé et al. 1987, Robin et al. 1996, Haywood et al. 1997. Website: http://www.obs-besancon.fr). In the latter only a mean extinction $\mathrm{A_V} = 0.7\,\mathrm{mag/kpc}$, associated with a widespread diffuse medium, is taken into account. The magnitude range selected for the comparison ($16.5 < \mathrm{m_B} < 21.25$) was choosen so as to stay within the completeness limit of the images and exclude saturated stars. Observations and the model (Fig. 5) match for $\mathrm{E(B-R)} = 0.31 \pm 0.03$ ($\mathrm{A_V} = 0.53 \pm 0.05\,\mathrm{mag}$) in the part of the optical images where $\mathrm{I}_\nu(100\,\mu\mathrm{m}) < 5.2\,\mathrm{MJy/sr}$ (pixels with $\Delta\mathrm{I}_\nu(100\,\mu\mathrm{m}) < 0$ in Fig. 4). The main peak in the B-R histogram is broader for the observations than for the model. It may be an effect of non-uniformity of extinction across the area.

The dashed line of Fig. 4 indicates the mean slope between $100\,\mu$m emission and $\mathrm{A_V}$ in the image: $\Delta\mathrm{I}_\nu(100\,\mu\mathrm{m})/\Delta\mathrm{A_V} = 5.5\,(\mathrm{MJy/sr})/\mathrm{mag}$. This value is significantly lower than the value of 18.6 MJy/sr/mag derived from the comparison of the $100\,\mu$m IRAS brightness with H I column densities in the Galactic Polar caps (Boulanger & Pérault 1988). The ratio 5.5 MJy/sr/mag corresponds to the mean slope of the $100\,\mu\mathrm{m} - \mathrm{A_V}$ relation over the A_V range 0.5 to 2 mag, while the Polar caps

Table 1. Summary of values used in the text fot the B, R, I bands

optical band	B	R	I
λ	4500	6500	9000
Polaris			
m_λ [a]	2.568	1.477	1.202
M_λ [b]	-3.44 ± 0.38	-4.36 ± 0.34	-4.55 ± 0.34
F_λ (MJy)[c]	$4.17\,10^{-4}$	$7.72\,10^{-4}$	$8.03\,10^{-4}$
F^0_λ (MJy) [d]	$6.03\,10^{-4}\ \pm 6\%$	$9.50\,10^{-4}\ \pm 3\%$	$9.17\,10^{-4}\ \pm 2\%$
L_λ (MJycm^2) [e]	$132.67 \pm 36\%$	$208.95 \pm 33\%$	$201.58 \pm 32\%$
F^0_λ/F^0_I	$0.66 \pm 6\%$	$1.04 \pm 3\%$	1
Interstellar grains			
A_λ/A_v [f]	1.34	0.75	0.48
ω_λ [g]	0.6	0.6	0.5
MCLD $123.5 + 24.9$ lowest column densities			
dS_λ/dI_{100}	$(2.4 \pm 0.2)\,10^{-3}$	$(4.3 \pm 0.1)\,10^{-3}$	$(3.0 \pm 0.1)\,10^{-3}$
dS_λ/dS_I	0.79 ± 0.2	1.42 ± 0.15	1
Low density medium illuminated by Polaris			
dS_λ/dS_I for $A_V \sim 0$ mag	2.2	1.95	1

[a] Arellano Ferro (1983a, 1983b)
[b] absolute magnitude for $A^0_V = 0.3 \pm 0.05$ mag and a parrallaxe $\theta = 7.56 \pm 0.48\,10^{-3}$ " (Hipparcos). We used: $M_\lambda = m_\lambda + 5\log\theta - 10 - A_\lambda$
[c] Polaris flux received on Earth. From m_λ values
[d] Polaris flux corrected from interstellar extinction
[e] Polaris luminosity
[f] Cardelli et al. (1989)
[g] albedos (Draine & Lee 1984).

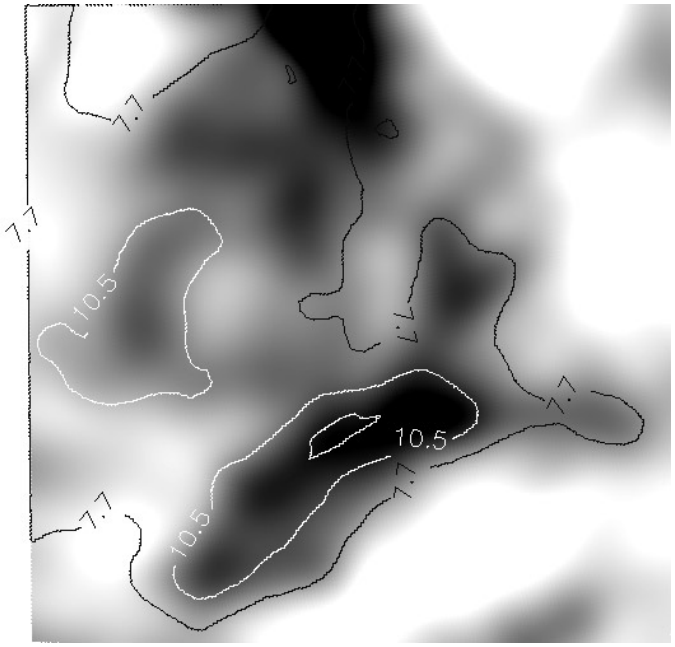

Fig. 3. Extinction map with $100\,\mu$m contours overlayed.

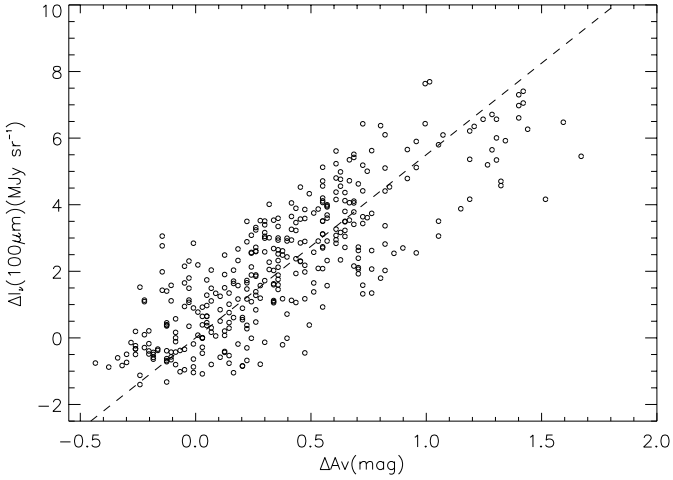

Fig. 4. Point to point comparison between $\Delta I_\nu(100\,\mu\mathrm{m})$ and ΔA_V. The plotted A_V and $100\,\mu$m values are computed with respect to the regions of lowest extinction and $100\,\mu m$ brightness in the field ($\Delta I_\nu(100\,\mu\mathrm{m}) = I_\nu(100\,\mu\mathrm{m}) - 5.2\,\mathrm{MJy/sr}$). Based on the comparison of stellar colors with those of the Besançon Galactic model (Fig. 5), we estimate the total cloud A_V to be $\Delta A_V + 0.53\,\mathrm{mag}$. The dashed line represents a ratio of 5.5 (MJy/sr)/mag.

value applies to $A_V < 0.4$. Due to the attenuation of the stellar radiation heating the dust, for clouds with significant extinction such as MCLD $123.5 + 24.9$, the $100\,\mu\mathrm{m} - A_V$ relation is expected to flatten with increasing A_V. This flattening has been observed for various clouds, in particular the Chamaeleon clouds (Boulanger et al. 1998). The Polaris $\Delta I_\nu(100\,\mu m)/\Delta A_V$ value is close to the mean value of 7.5 MJy/sr/mag determined for the Chamaeleon clouds over the A_V range 0 to 2 mag.

On the magnified infrared images, two main regions (each one being delimited by a 11 MJy/sr $100\,\mu$m contour) are remark-

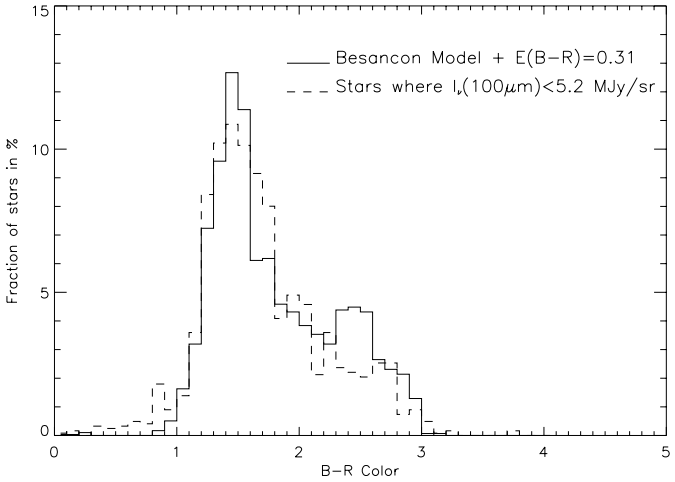

Fig. 5. Comparison of (B-R) histograms for the Besançon Galactic model and the stars observed where $\mathrm{I}_\nu(100\,\mu\mathrm{m}) < 5.2\,\mathrm{MJy/sr}$. The stars of the simulated stellar catalog, have all been reddened by E(B-R)=0.31. With Cardelli et al. (1989) extinction curve ($\mathrm{R_V} = 3.1$), this yields $\mathrm{A_B} = 0.69$. Histograms were built for stars in the blue magnitude range $16.5 < \mathrm{m_B} < 21.25$.

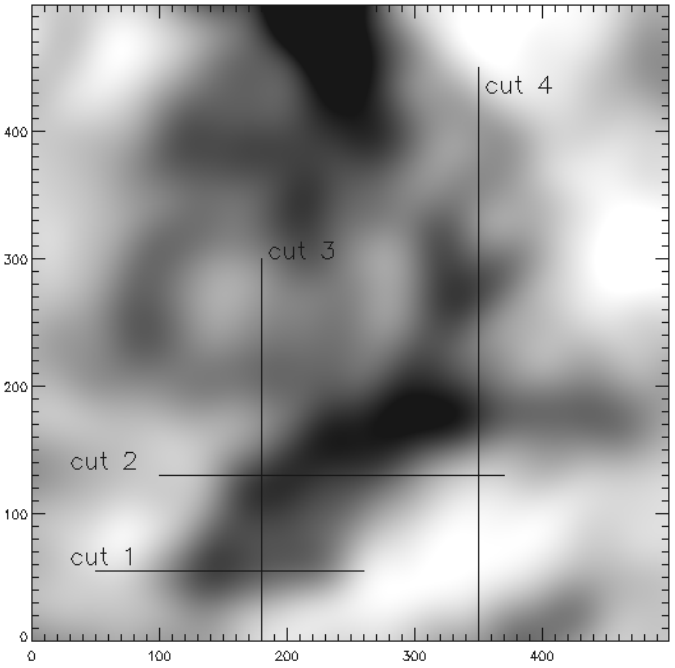

Fig. 6. R image smoothed to IRAS resolution. Numbers on each side of the image refer to pixel numbers so that the reader can easily find the pixel position in the cuts of Fig. 7.

able. Region I is a slightly curved filament at the southern part of the field, about 12′ large. This feature gives rise to the most spectacular part of the optical images and dominates the emission at $100\,\mu$m. It gradually vanishes at shorter wavelengths. Region II, to the North-West of region I, has a more circular shape and dominates the $60\,\mu m$ image. Großmann et al.'s (1990) study of the region shows that column densities, and probably gas density, are much higher in region I than in region II. Both regions are detected in ^{12}CO emission while only region I is detected in ^{13}CO and H_2CO.

We made a point to point comparison of IRAS $100\,\mu$m and $60\,\mu$m emissions over regions I and II and on the more diffuse part of the cloud. We find a mean ratio of 0.13 on both region II and the diffuse cloud. Over region I this ratio is much lower and falls to about 0.03.

3.2. Visible images

Figs. 1 and 2 show a clear similarity between the optical images (B, R and I) and the $100\,\mu$m image. Similarity between the optical and far-infrared brightness of high latitude cirrus clouds was first pointed out by de Vries & Le Poole (1985). They showed that for low extinctions both the optical and far-infrared brightness increase with dust column density. Due to extinction this relation progressively flattens for increasing column densities. For even higher column densities, absorption is the dominant process and we can expect the optical emission to decrease. In the study of de Vries and Le Poole, little increase in the B cloud brightness is observed for $\mathrm{A_V} > 0.7$. Brightness flattening and decrease are also expected in the R and I bands but at larger $\mathrm{A_V}$. For the $\mathrm{R_V} = 3.1$ extinction curve, the B magnitude threshold of de Vries and Le Poole scales to 1.2 and 1.9 in R and I. The attenuation of stellar radiation by dust absorption also introduces a progressive flattening of the $100\,\mu m$ brightness - $\mathrm{A_V}$ relation (see Sect. 3.1). Empirically, little increase of the $100\,\mu$m cloud brightness is observed for $\mathrm{A_V} > 2$ (e.g. Boulanger et al. 1998).

A diagram of the optical B, R or I emissions versus the IRAS $100\,\mu$m brightnesses should reflect the correlation with dust column density and depend on the relative threshold at which the brightness saturates. Because the optical emission saturates and decreases before the $100\,\mu$m emission, the slope $\mathrm{d}S_\lambda/\mathrm{d}I_{100}$ is expected to decrease with increasing column density. Such a comparison between optical and far-infrared data may not be so straightforward. When structures with different optical depths lie on the same line of sight, which is presumed to be the most common case, a plot of optical emission versus the $100\,\mu$m brightness is expected to be more complicated. This might explain the large dispersion such plots usually show (see Guhathakurta & Tyson 1989).

A point to point comparison over large regions of the optical image is also unreliable and difficult to analyze due to the large scale straylight which we only approximately subtracted from the optical images (Sect. 2.2). Residuals of scattered light in the Earth's atmosphere introduce a variable offset on low spatial frequencies. To overcome this problem, we chose to compare local brightness variations along cuts through region I (see Sect. 3.1). Fig. 7 shows that locally it is possible to linearly match the R emission to the $100\,\mu$m emission. The proportionality coefficients, written above each cut, measure the local slope of R versus I_{100}, $\mathrm{d}S_R/\mathrm{d}I_{100}$. If Fig. 6 is used to compare the coefficient value and the corresponding region along the cut, it is clear that $\mathrm{d}S_R/\mathrm{d}I_{100}$ tends to decrease when going into region I known, from molecular observations (Sect. 3.1), to be the densest part of the cloud. As already discussed, this is the behaviour expected

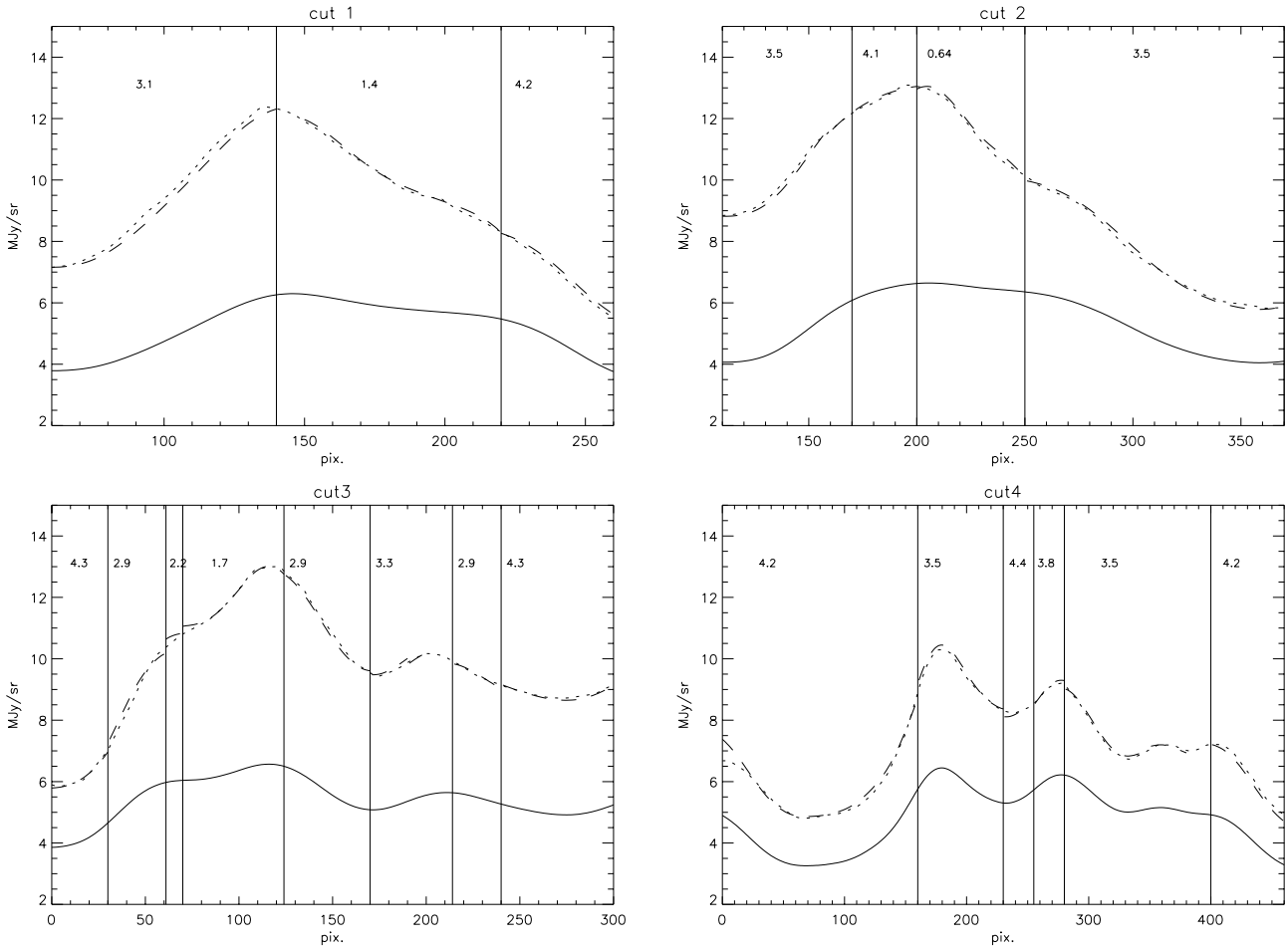

Fig. 7. Comparison of R and $100\,\mu$m emission along the 4 cuts drawn in Fig. 6. For each cut, the dotted curve is the IRAS $100\,\mu$m brightness. R band surface brightness, smoothed at IRAS resolution, is overlaid in dashes. It was first linearly transformed (divided by $\mathrm{dS}_R/\mathrm{dI}_{100}$ and an appropriate offset) so as to match the $100\,\mu$m emission. This scaling was done independently within each of the intervals separated by vertical lines. In each interval, the local value of $10^3\mathrm{dS}_R/\mathrm{dI}_{100}$ is written on the top of the plot. The offset applied to the R band brightness is not represented. The solid line at the bottom of each graph is the R brightness multiplied by 155, with an arbitrary offset.

from absorption effects. Column densities variations in the regions of lowest column density should correspond to the maximum value of $\mathrm{dS}_R/\mathrm{dI}_{100}$. We find $\mathrm{dS}_R/\mathrm{dI}_{100} \sim 4.3\,10^{-3}$ in the low density medium of MCLD 123.5+24.9. There is no straigthforward correspondence between the absolute R surface brightness and the $100\,\mu\mathrm{m}$ emission: regions of low optical depth usually correlate with a minimum in the infrared emission, but not necessarily with low $100\,\mu\mathrm{m}$ values: our relation concerns the variations of those emissions, not the emission themselves. This can be explained if mediums of different optical depths coexist on the same line of sight, and is clearly related to the structure of the interstellar medium. This problem will be treated in more detail in a forthcoming paper (Zagury, in preparation).

The same comparison between B and IRAS $100\,\mu$m is not as easy to arrive at, which we interpret as a result of extinction, much higher in the B band (a factor of 2, see Table 1) than in the R band. Up to reasonably high column densities, the $100\,\mu$m emission is proportionnal to the column density while B emission saturates for lower $\mathrm{A_V}$ than does the R emission. Scattered emission in the R and I bands will follow the $100\,\mu$m emission farther along than it will in the B band. We could only determine $\mathrm{dS}_B/\mathrm{dI}_{100}$ in the most diffuse part of the cloud. We find $\mathrm{dS}_B/\mathrm{dI}_{100} = 2.4\,10^{-3}$. This value was confirmed by comparing cuts in the B and R unsmoothed images across the faintest structures.

Stars were not subtracted from the I image since this image was obtained late after this work began. Consequently it was also not smoothed to the IRAS resolution. But, from a comparison of the R and I images, we find $\mathrm{dS}_I/\mathrm{dI}_{100} = 3\,10^{-3}$. Proportionality coefficients between optical and IRAS $100\,\mu$m images are reported in Table 1.

4. Estimation of MCLD 123.5 + 24.9 distance to the sun

In this paper, we assume that MCLD 123.5+24.9 and more generally the Polaris Flare are in front of the North star. In Appendix A, we present and discuss various attempts made at determining the extinction of Polaris. Discussions on the star colors are inconclusive and the most convincing argument for

reddening is the fact that Polaris light is polarised (Axon & Ellis 1976). Polaris parallax, given by Hipparcos, leads to a distance of 133 ± 8 pc from the Sun to Polaris. The star contribution to the Polaris Flare heating is expected to be negligeable, compared with that of the ISRF, because no emission enhancement nor 60 to $100\,\mu$m color gradient toward the star can be seen on IRAS images. Further, the $I_\nu(100\,\mu\mathrm{m})$ over A_V ratio (Sect. 3.1) for MCLD 123.5+24.9 fits with what is expected from ISRF heating, with no local enhancement. Polaris spectrum is very similar to that of the Sun (Sanwal et al. 1988, Arellano Ferro 1984) with a temperature of ~ 6000 K. Its power is mainly concentrated in the optical wavelengths and peaks at 5000 Å. Mathis et al.'s (1983) model of grain properties, absorption cross sections and albedos, was used to estimate the power absorbed by dust from ISRF heating and from heating by Polaris at a given distance, r, to the star. It was found that both are equal at $\sim$2 pc to the star. Polaris heating decreases as $1/r^2$ and is $\sim 1/10$ of the ISRF at 6 pc. So a minimum distance from Polaris to the Polaris Flare of ~ 6 pc seems reasonable. This leads to a distance from the Polaris Flare to the Sun of less than ~ 125 pc and a z-distance to the Galactic plane of less than 50 pc.

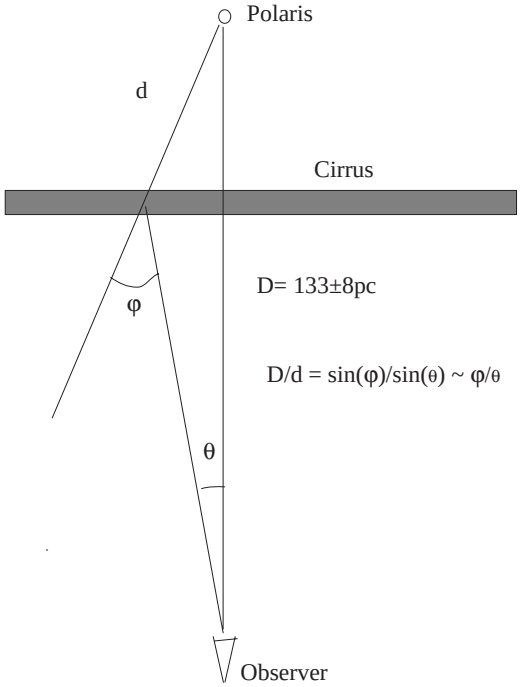

Fig. 8. Schematic view of the relation between Polaris, MCLD $123.5+24.9$, and the observer.

5. Possible illuminating sources of MCLD $123.5 + 24.9$

The diffuse emission of MCLD $123.5 + 24.9$, which can be surmised from Palomar plates, was attributed by Großman et al. (1990) to scattered light from the Galactic Plane. ISRF is naturally thought of as a possible source of the optical emission. However, as shown in the following paragraph, the idea of back scattering of Galactic starlight, as originally proposed by Sandage (1976) do not apply to cirrus clouds close to the Sun.

An important key to the understanding of optical interstellar emission is the strongly forward scattering property of interstellar dust. Most of HLCs are believed or proved to be close to the Sun ($d < 200$ pc, with an average of 100 pc, see Magnani & de Vries 1986). Some, like MBM 12 (Hobbs et al. 1986), are as close as $d \sim 60$ pc. The z-distance of those clouds is small compared to the scale height of stars (several 100 pc) and there is a comparable amount of light illuminating the front and back sides of one such cloud. The dense core in MCLD $123.5+24.9$ studied by Falgarone et al. (1998) is seen in absorption (the white bar on the lower left hand part of the B image in Fig. 2) on the optical images. Many extinct features are observed in absorption on the Palomar plates (Lynds 1962) at high galactic latitudes. In the case of isotropic scattering, Sandage (1976) has calculated that a low density medium (a fortiori this must be true for a cloud core of higher column density) illuminated by the Galactic plane will give a reflected optical emission detectable in the Palomar plates. If interstellar dust was not strongly forward scattering one should see reflected light from the previous opaque structures, which is not the case. Thus, interstellar dust must be strongly forward scattering light. A similar conclusion was reached by Henyey & Greenstein (1941) in their study of the diffuse optical emission in the Galaxy and by Mattila (1971) for dark clouds. Both authors find a high assymetry factor ($g_0 > 0.8$, see Sect. 6). The forward scattering nature of interstellar grains has never been contradicted by following studies. For instance, studies of opaque globules (e.g Witt & Stephens 1974, FitzGerald et al. 1976) find that their limb brightened emission implies a strongly forward scattering function with $g_0 > 0.7$.

In the following sections, we show that the optical emission of MCLD $123.5 + 24.9$ can be explained by illumination by the brightest star in the cloud neighbourhood, the North star. Polaris, a F red giant Cepheid, is only one degree away from the field. Its properties and magnitude in the various bands are well known (Arellano Ferro 1983a, 1983b, see Table 1).

For Polaris to illuminate the cirrus, 3 constraints have to be dealt with:

- the distance between Polaris and MCLD $123.5 + 24.9$ has to be such that the star radiation field is strong enough to explain the measured optical emission in MCLD $123.5 + 24.9$
- but weak enough for the heating of dust to be negligeable compared to that of the ISRF.
- The colors of Polaris light scattered by the lowest column density parts of MCLD $123.5+24.9$ have to match the cloud colors derived in Sect. 3.2. (see Table 1).

These points shall be discussed in the next section.

6. Model for scattering in a medium of low optical depth

To compare observed intensities and colors (Table 1) of MCLD $123.5 + 24.9$ to those expected from Polaris scattering, we need a simple model of light scattering which is described hereafter.

For $\tau \ll 1$ multiple scattering may be neglected. The light in direction $\varphi \neq 0$ (Fig. 8) is deflected from the incident radiation field direction after only one scattering.

At optical depth $\tau_0 < \tau$ the incident radiation field is diminished by a factor $e^{-\tau_0}$ and between τ_0 and $\tau_0 + d\tau$, $\mathrm{g}(\varphi)\, e^{-\tau_0} d\tau$ of it is removed to direction φ (per steradian). g is the scattering phase function, usually assumed to be the Henyey Greenstein function defined by:

$$g(\varphi) = \frac{(1-g_0^2)}{4\pi(1+g_0^2-2g_0\cos\varphi)^{1.5}} \quad (1)$$

where $g_0 = < g(\varphi)\cos(\varphi) >$ is the only free parameter of this function. $g_0 = 0$ corresponds to isotropic scattering and $g_0 = 1$ to complete forward scattering.

Only a fraction $e^{-(\tau-\tau_0)}$ of the scattered beam at τ_0 will reach the observer. So the fraction of the incident light scattered from the original beam into direction φ shall be:

$$\int_0^\tau e^{-(\tau-\tau_0)} \mathrm{g}(\varphi)\, e^{-\tau_0} d\tau = \tau e^{-\tau} \mathrm{g}(\varphi) \quad (2)$$

If the source radiation field is F_λ^1 (MJy) at the back surface of the cloud and the power received on Earth S (MJy/sr), this gives:

$$\mathrm{S} = \mathrm{F}_\lambda^1 \tau e^{-\tau} \omega \mathrm{g}(\varphi) \quad (3)$$

ω is the albedo.

The slope of $\mathrm{S}(\tau)$ is:

$$\frac{\mathrm{dS}}{\mathrm{d}\tau} = \mathrm{F}_\lambda^1 \omega \mathrm{g}(\varphi)(1-\tau) e^{-\tau} \quad (4)$$

If 2 different wavelenghts λ_1 and λ_2 are considered, the slope of S_{λ_1} versus S_{λ_2} is:

$$\begin{aligned} \frac{\mathrm{dS}_{\lambda_1}}{\mathrm{dS}_{\lambda_2}} &= \frac{(\mathrm{dS}_{\lambda_1}/d\tau_{\lambda_1})}{(\mathrm{dS}_{\lambda_2}/\mathrm{d}\tau_{\lambda_2})} \frac{\mathrm{A}_{\lambda_1}}{\mathrm{A}_{\lambda_2}} \\ &= \frac{F_{\lambda_1}^1}{F_{\lambda_2}^1} \frac{(1-\tau_{\lambda_1})\, e^{-\tau_{\lambda_1}}}{(1-\tau_{\lambda_2})\, e^{-\tau_{\lambda_2}}} \frac{\mathrm{A}_{\lambda_1}}{\mathrm{A}_{\lambda_2}} \frac{\omega_{\lambda_1}}{\omega_{\lambda_2}} \frac{\mathrm{g}_{\lambda_1}(\varphi)}{\mathrm{g}_{\lambda_2}(\varphi)} \end{aligned} \quad (5)$$

Because: $\mathrm{d}\tau_{\lambda_1}/\mathrm{d}\tau_{\lambda_2} = \mathrm{A}_{\lambda_1}/\mathrm{A}_{\lambda_2}$.

This model is adapted to the situation where all light in direction φ is deflected from the source without any contribution of light coming from other angles. That is when τ is small enough for one to neglect multiple scattering. This implies $A_V << 1$. The model should be adapted to our study of the low column density medium of MCLD $123.5 + 24.9$.

Fig. 9 illustrates the model just described with $\mathrm{g}_0 = 0.8$, $\varphi = 20°$, a unit source radiation field for each wavelength ($F_\lambda^1 = 1$), albedos and A_λ-values given in Table 1. We assume same phase function for all wavelengths. The left hand plot, shows S_{λ_2} versus S_{λ_1} with parameters corresponding to $\lambda_2 = B$ and $\lambda_1 = R$. Slopes of $dS_{\lambda_2}/dS_{\lambda_1}$ versus A_V will not depend on the phase function (Eq. 5) and are shown on the right hand plot, for the different optical bands. They vary steeply with increasing optical depth. At $\tau_B = 0.37$ ($\tau_R = 0.67$, $\mathrm{A_V} = 0.5$) the slope $\mathrm{dS_B}/\mathrm{dS_R}$ has already decreased more than 50% from its value at the origin.

7. Can Polaris illuminate MCLD 123.5 + 24.9?

7.1. Strength of the expected optical emission at a given distance to the star

7.1.1. Maximum of emission over the field

MCLD $123.5{+}24.9$ surface brightness, S_λ, should be maximum for τ-values a little bit higher than 1, before absorption starts dominating further scattering.

A lower limit of $0.37\omega F_\lambda^1 g(\varphi)$ for the maximum possible surface brightness ($S_{\lambda,max}$) of MCLD $123.5 + 24.9$ can be derived using the model of Sect. 6.1 which takes into account only photons scattered once. $F_\lambda^1 = F_\lambda^0 (D/d)^2$ (see Fig. 8 and Table 1) is Polaris flux at wavelength λ and at the cloud location.

$S_{\lambda,max}$ will always be less than the extension of a very low opacity medium to higher τ values (given by the dotted line going through the origin in Fig. 9). Thus, taking $\tau \sim 1$, we find $S_{\lambda,max} < \omega F_\lambda^1 g(\varphi)$.

Hence, the maximum possible surface brightness of the cirrus should be in the range:

$$\begin{aligned} S_{\lambda,max} &= (0.7 \pm 0.3)\omega F_\lambda^1 g(\varphi) \\ &= (0.7 \pm 0.3)\omega F_\lambda^0 (D/d)^2 g(\varphi) \end{aligned} \quad (6)$$

Free parameters in Eq. 6 may be reduced using $D/d = \sin\varphi/\sin\theta$ (see Fig. 8) and $\theta \sim 1.5°$. F_λ^0 is taken from Table A.1.

Fig. 10 plots $S_{\lambda,max}$ (Eq. 6) in the R (or I band) for different values of g_0 and for $\omega = 0.6$. For both R and I bands, the maximum surface brightness found on the image is $\sim 0.032 \pm 0.003$ MJy/sr. The possible range of values for the maximum emission over MCLD $123.5 + 24.9$, imposed by the observations, is between the 2 horizontal lines.

Considering the minimum distance between Polaris and MCLD 123.5+24.9, set by IRAS data (Sect. 4), Polaris appears as a plausible source of the optical emission for g_0 values larger than 0.6. For $g_0 = 0.8$, the distance d between the cloud and Polaris should satisfy $0.05 < d/D < 0.2$, or, for $D = 130$ pc: $6.5 < d\,(\mathrm{pc}) < 25$.

7.1.2. Optical emission of the low density medium

The possible illumination by Polaris can also be tested using the emission of the lowest column density parts of the cloud. The surface brightness of this medium should be well approximated by Sect. 6 model.

Using the formal expression of $S_{R,max}$ (Eq. 6), Eq. 4 applied to the R band can be written as:

$$\frac{\mathrm{d}S_R}{\mathrm{d}\tau_R} = \frac{S_{R,max}}{0.4}(1-\tau_R)\, e^{-\tau_R} = 0.085\,(1-\tau_R)\, e^{-\tau_R}, \quad (7)$$

because $S_{R,max} \sim 0.032$ MJy/sr (Sect. 7.1.1).

For the lowest column density parts of the R image, $\mathrm{dS}_R/\mathrm{d}\tau_R = (\mathrm{dS}_R/\mathrm{dI}_{100})(\mathrm{dI}_{100}/\mathrm{dA}_V)(\mathrm{dA}_V/\mathrm{d}\tau_R) = 0.034$ MJy from the observational values in Table 1 and Sect. 3.1.

For $\mathrm{dS}_R/\mathrm{d}\tau_R = 0.034$ MJy, Eq. 7 is solved by $\tau_R \sim 0.4$. This gives $\mathrm{A}_V \sim 0.5$ in the low density medium of the cloud,

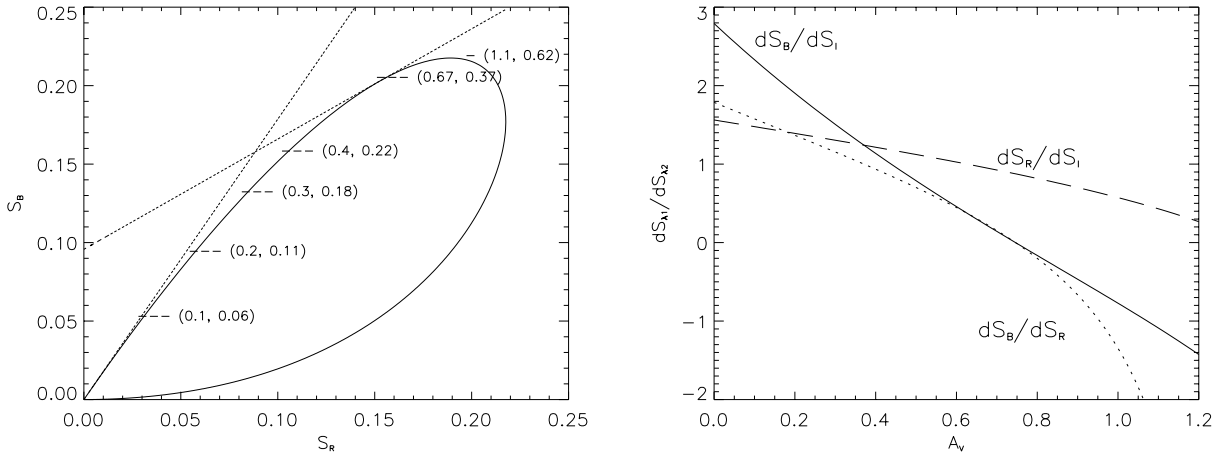

Fig. 9. *Left*: Expected color diagram of the scattered emission for the B and R bands. The source radiation field is supposed to be 1 unit of power per unit surface, and S_R and S_B are surface brightness in the same power units by sr. Albedos and relative τ-values are given in Table 1 and $g_0 = 0.8$. Slopes at the origin and at $\tau_V = 0.5$ ($\tau_R = 0.37$ and $\tau_B = 0.67$) have been traced (dotted lines). Values in parenthesis are (τ_B, τ_R) along the curve. The corresponding A_V value is in between those 2 values. *Right*: slopes variations as a function of A_V. Slopes have a steep decrease with increasing optical depth.

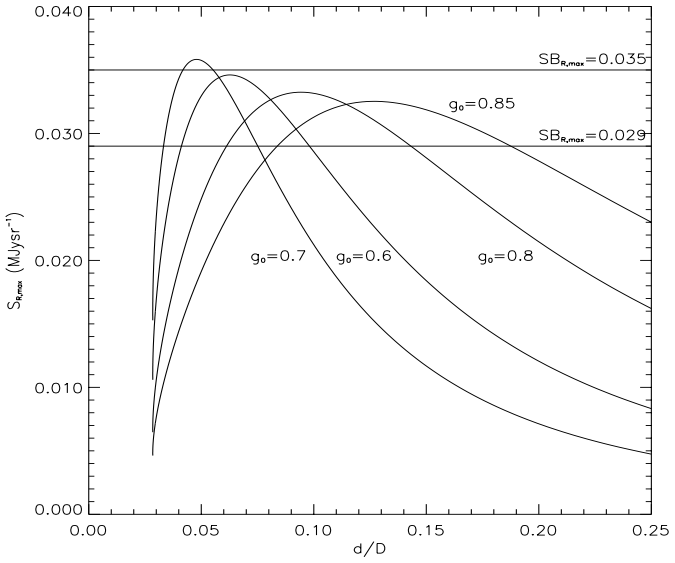

Fig. 10. Maximum of MCLD $123.5 + 24.9$ emission in the R band. The curves are $S_{R,max}$, from Eq. 6 for different values of g_0. The 2 lines show the range of values of $S_{R,max}$ which can be infered from the R band observations.

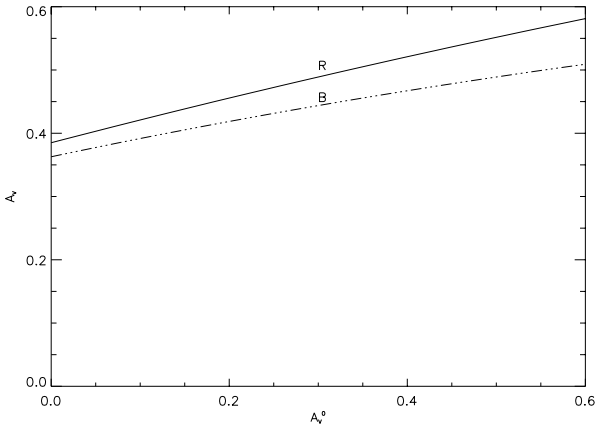

Fig. 11. A_V values of MCLD $123.5 + 24.9$ versus A_V^0, effective extinction in Polaris direction in the V band. Each 'R band' and 'B band' curve corresponds to the A_V versus A_V^0 curve found using respectively the dS_B/dS_I and dS_R/dS_I ratios. They are close enough to justify possible illumination by Polaris.

in agreement with our estimate of the minimal extinction in the field obtained from stellar reddenings (see Sect. 3.1).

7.2. Comparison of observed and expected optical colors of MCLD $123.5 + 24.9$

The last line of Table 1 lists B/I and R/I colors expected for a low column density cloud illuminated by Polaris ($S_\lambda/S_I = \omega_\lambda A_\lambda F_\lambda^0/\omega_I A_I F_I^0$, λ designs the B or R band in the following). F_λ^0, in Table 1 was calculated for a Polaris reddening $A_V^0 = 0.3$ (see appendix). If Polaris was not reddened ($F_\lambda^0 = F_\lambda$ in Table 1) the expected colors of a low column density medium illuminated by Polaris would be $S_B/S_I = 1.7$ and $S_R/S_I = 1.8$. In both cases the computed colors are significantly bluer than the observed one. From similar comparisons Guhathakurta & Cutri (1994) concluded that the colors of cirrus clouds implied significant luminescence in the R and I bands. We show here that the colors of MCLD $123.5+24.9$ can be explained by extinction effects with no need of luminescence.

The optical colors derived in Sect. 3.2 are not the ratio between the total surface brightnesses S_λ for B, R and I bands but the slope of the non-linear relation between these surface brightnesses, at the non zero optical depth of the lowest column density parts of the cloud. From stellar reddenings, the minimum extinction in the optical field was estimated to be $A_V \sim 0.5$ (Sect. 3.1). Fig. 9 shows that the slope dS_λ/dS_I at $A_V \sim 0.5$ can be considerably attenuated from its value at $A_V = 0$.

The cirrus surface brightness at a given wavelength is proportional to the source radiation field flux, F^1_λ, at the cloud location and to the scattered emission in direction φ for a unit source radiation field: $\mathrm{S} = \mathrm{F}^1_\lambda\,\mathrm{S}_{\mathrm{sca},\lambda}$. With Sect. 6 modelling: $\mathrm{S}_{\mathrm{sca},\lambda} = \omega_\lambda \tau_\lambda \mathrm{e}^{-\tau_\lambda} \mathrm{g}_\lambda\,(\varphi)$.

The slope of B or R versus I surface brightnesses is: $\mathrm{dS}_\lambda/\mathrm{dS}_\mathrm{I} = F^1_\lambda/F^1_I dS_{sca,\lambda}/dS_{sca,I} = F_\lambda/F_I e^{0.92A^0_V(\alpha_\lambda - 0.48)}$ $dS_{sca,1}/dS_{sca,I}$, with notations of Table 1: F_λ is Polaris flux measured on Earth, A^0_V is Polaris reddening, $\alpha_\lambda = A_\lambda/A^0_V$ (Table 1).

Hence:

$$\mathrm{A}^0_\mathrm{V} = \frac{\lg(\frac{\mathrm{dS}_\lambda}{\mathrm{dS}_\mathrm{I}}\frac{\mathrm{F}_\mathrm{I}}{\mathrm{F}_\lambda}) - \lg(\frac{\mathrm{dS}_{\mathrm{sca,I}}}{\mathrm{dS}_{\mathrm{sca},\lambda}})}{\alpha_\lambda - 0.48} \tag{8}$$

In the right hand term, $\mathrm{dS}_\lambda/\mathrm{dS}_\mathrm{I}$ and $\mathrm{F}_\mathrm{I}/\mathrm{F}_\lambda$ are observed values given in Table 1. $\mathrm{dS}_{\mathrm{sca,I}}/\mathrm{dS}_{\mathrm{sca},\lambda}$ is a function of the A_V value in MCLD $123.5+24.9$. Its variations with A_V are shown in the right hand plot of Fig. 9. Using Eq. 8, A_V versus A^0_V is plotted Fig. 11, in the approximation of the single scattering model of Sect. 6.

For each B-I and R-I color, Fig. 11 shows the combination of A_V (the diffuse medium extinction) and A^0_V (Polaris extinction) values for which the model prediction agrees with the observed colors. We assumed the phase function to be identical in the three bands and used the albedo values, ω, given in Table 1. Uncertainties in the curves of Fig. 11 come from the parameters of the model (albedos, $\mathrm{A}_\lambda/\mathrm{A}_\mathrm{V}$, variation of g with wavelength) and the single scattering assumption. The contribution of multiple scatterings to the observed brightnesses increases with opacity and thus from the I to the B band. It will make the predicted colors bluer and will shift the B and R band curves towards higher A_V. Together with uncertainties on the dust parameters, this could account for the slight shift between the two curves.

The extinction over the lowest column density parts of the optical image was estimated to be ~ 0.5 mag (Sects. 3.1 and 7.1.2). For this value of A_V, Fig. 11 shows that observed and computed colors match at $A^0_V \sim 0.35$, a value within the range of possible Polaris extinction ($0.08 < A^0_V < 0.4$ see Appendix). In our modelling, this value should be considered as an upper limit of Polaris reddening: taking multiple scattering into account will diminish A^0_V. Thus, within the limitations and uncertainties of the model, we consider that the optical colors of MCLD $123.5 + 24.9$ low density medium can be explained by illumination by Polaris for all possible A^0_V values.

8. Conclusion

We have presented B, R, I images of a cirrus with ~ 2" (10^{-3} pc at 100 pc) resolution and $1^\circ \times 1^\circ$ field of view. Study of the infrared emission shows that the cirrus is heated by the ISRF. But absorption features in the optical image and the small z-value of the Polaris Flare lead us to believe that the light source responsible for the spectacular feature seen in Fig. 1 is behind the cloud. In the present paper we have investigated the possibility for the North star, 1° North to the field, to be the source of illumination. Assuming forward scattering ($g_0 \sim 0.8$), for a distance of the star to the cloud between 6 and 25 pc Polaris does not contribute to dust heating but is luminous enough to explain the observed cloud surface brightness in the optical.

The cloud colors, B-I and R-I, are redder than scattered light by a medium of optical depth close to 0 (Table 1). However CCD images from ground based telescope do not provide the absolute cloud surface brightnesses. For our data and comparable studies (e.g. Guhathakurta & Tyson 1989), the reported colors are the ratio of local brightness gradients, on angular scales smaller than the overall extent of the cirrus cloud. We have shown that colors such defined depend strongly on the range of cloud optical depths over which they are derived. In practice, they are significantly redder than the colors which would be determined from the ratios of the full cloud brightnesses. Polaris scattered light will explain the colors of the cloud's lowest density parts for an $\mathrm{A}_V \sim 0.5$ mag. This value was independently confirmed by a study of stellar reddenings. The low density approximation, which consists of assimilating the color slope to that at $\mathrm{A}_\mathrm{V} = 0$ cannot be applied. This has never been taken into account in previous studies. Our interpretation gives a natural explanation of MCLD $123.5+24.9$ colors with no need of red luminescence.

If Polaris is indeed the illuminating source of MCLD $123.5 + 24.9$ it might also illuminate other parts of the Polaris Flare and perhaps be responsible for all the optical emission, surmised on Palomar plates, of the region.

The reflexion initiated in this paper has two clear outcomes. First it shows the need to reconsider the origin (the illumination source) of the optical emission of high latitude clouds. Preceding studies have always assumed this radiation field to be the Galactic plane or the ISRF. If the optical emission of MLCD - which is after all a cirrus with properties very similar to other cirrus - is explained by a background source, with no need of red luminescence, why should other cirrus be so different? The illumination of cirrus at optical wavelengths will be discussed in a forthcoming paper.

Secondly, it seems clear that the information contained in Fig. 1 was very roughly, and only slightly used in the present study. CCDs are sensitive enough to provide deep, high resolution, images of interstellar clouds with much more detail than previously done in Palomar plates for instance. In future papers we wish to develop tools and a general framework to understand the implications of high resolution optical images for grain properties and for the small scale structure of the interstellar medium.

Acknowledgements. Vincent Banchet and Frédéric Zagury started this work during their PhD thesis and were financially supported by the French National CIFRE grant and CYBEL multimedia company. We wish to thank Gerard Chevalier and all the persons working at CYBEL for the help provided during those years. This work was finished at Nagoya University under the Japan Society for the Promotion of Science grants ID N° P97234 (F.Z) and ID N° RC19833013 (F.B). We wish to thank JSPS, Professor Y. Fukui, and all the Radio-Astronomy group of Nagoya University for the generous hospitality and the full support received during this stay.

Table A.1.

Star	HD	DM		E_{B-V}			E_{V-I}	distance to the Sun		Sp. Type*		$IRAS_{100\,\mu m}$
			GF	H[a]	S[a]		H	GF	H	GF	S&H	
				mag			mag		pc			MJy/sr
1	*6369*	*+87°*	*009*	*0.02*		*0.07*		*185*		*A*	*F5*	*7.62*
2[b]	11696		015	0.02	0.16	0.42	0.17	157	155±15	A	A3	7.86
3	*12364*		*016*	*0.01*		*<0.1*		*118*		*F*	*G0*	*10.80*
4	*26341*		*033*	*0.03*	*0.01*	*0.35*	*-0.14*	*144*	*263±51*	*A*	*F2*	*6.79*
5	5914	+88°	004	0.03	0.03	0.03	0.01	99	98.7±4.8	A	A3V	4.60
6	14369		009	0.03	0.1	0.1	0.01	76	88.4±4.9	F	F0	6.17
7	17376		013	0.07		> 0.2		138		A	A	7.54
8	211455		131	0.00	0.09	0.65	0.47	166	250±45	A	A5	6.22
9			*134*	*0.00*		*0.1–0.4*		*292*		*A*	*G5*	*2.6*
10	21070	+89°	003	0.17	0.15	0.35	0.12	125	150±18	A	A5	6.10
11			*038*	*0.30*		*0.1*		*625*		*B*	*A0*	*4.82*
		Polarization										
		Q_{Stokes}	U_{Stokes}									
12[b]	26356	0	0		0.06	0.06	0.13		215±30		B5V	2.49
13	Polaris	-0.00135	-0.00173	0				110	133±9		F7:Ib-IIv	5.80

* star-lines for which GF's spectral type is not in agreement with Simbad/Hipparcos are in italic.
[a] E_{B-V} and E_{V-I} using Hipparcos (H) or Simbad (S), and $(B-V)_0$ from FitzGerald (1970) or Johnson (1966). Hipparcos and Simbad do not allways give the same (B-V) value, probably because Hipparcos uses Helmer et al. (1983) V magnitude.
[b] variable star.

Appendix A: on the reddening of the North star

A.1. Introduction

The reddening of the North star is an important issue to both Cepheïd models (for distance estimates) and to studies of the interstellar medium. Early studies of Polaris reddening (Kraft 1960, Fernie 1966) concluded that the star is slightly reddened. Since 1968, those studies have been criticized and recent papers accord no reddening to the star. Reviews on the subject can be read in Parsons & Bouw (1971), Gauthier & Fernie (1978, hereafter GF), Feltz & McNamara (1980), Turner et al. (1987) and Fernie (1990). Of special interest is the study by GF which emphasizes how difficult it is to prove the reddening of Polaris by examining Polaris' spectroscopic features (Kraft 1960, Fernie 1966) known to have peculiarities, and also by examining Polaris' star companion, Polaris B (see Turner 1977) which suffers from straylight contamination from Polaris. GF have analysed the reddening of 11 stars within 1° to Polaris through Stromgren photometry. They conclude Polaris is unreddened and estimate a distance of ~ 110 pc from the star to the Sun using Turner's (1977) estimation of the star visual absolute magnitude ($3.45 \pm .25$ mag).

Recent interest in this question has been sparked by studies of the Polaris Flare (Heithausen & Thaddeus 1990). If Polaris is reddened, the star is most likely to be behind the cirrus. It is then possible to estimate the cloud distance and the scale at which structures are observed, along with quantities such as the total mass of the Cirrus (Meyerdierks & Heithausen 1996).

In their most recent papers (after 1992) on the Polaris Flare, Heithausen et al. assert that Polaris is behind the Cirrus and use GF estimations of Polaris' distance to derive that of the Polaris Flare. This may contradict the argument of GF, that Polaris is unreddened.

Polaris distance derived by GF is less than Hipparcos (Table A.1) which can be accounted for by some reddening in the star direction and indicate some bias in GF analysis. If the star really is at 130 pc, the correction which should be applied to GF estimate of Polaris reddening is $A_V^0 \sim 0.5$ mag, the same value as found for MCLD123.5+24.9 low density medium. We tried to reanalyze GF results using the most recent data in the Simbad and Hipparcos databases. The comparison shows that stars at a greater distance than ~ 150 pc and perhaps as close as 100 pc to the Sun, might well be reddened. Polaris, at a distance of 133 ± 9 pc to the Sun can be reddened which would be supported by the measured polarisation of Polaris (Axon & Ellis 1976).

Concerning our work, Polaris extinction (A_V^0) enters in the comparison of observed and computed colors (Sect. 7.2) but not in a very critical manner. Only the relative position of the star and MCLD123.5+24.9 has critical importance. Because dust strongly scatters light in the forward direction, if the star is in front of the cirrus, illumination of MCLD123.5+24.9 by Polaris would have to be abandonned. Any significant reddening of the star would greatly enhance the reliability of the present paper.

A.2. Data analysis

Table A.1 presents the 11 stars used by GF to probe the non reddening of Polaris. The first column is the star number to be used hereafter. Column 2 and 3 are HD and DM names for each

star. In the following column we give the reddening E_{B-V} of each star from GF, Simbad, and Hipparcos when available. For stars in Hipparcos catalog an additional estimate of the reddening was obtained from the (V-I) color. Intrinsic B-V and V-I colors of stars are taken from FitzGerald (1970) or Johnson (1966). The error bar on B-V given in Hipparcos is always very small, less than 0.02 mag but, surprisingly, the agreement on B-V between Hipparcos and Simbad is sometimes poor. For stars (2), (4) and (8), Simbad B-V values are much larger than those of Hipparcos. This puts large uncertainties on those stars reddening. Distances to the Sun are given from GF and Hipparcos. When available, we consider Hipparcos distances to be the correct ones. Spectral types are given from GF and Simbad. The last column of Table A1 lists 100 μm IRAS brightnesses, indicative of the mean amount of matter associated with the Polaris Flare, over a $5'$ beam, at the position of each star. In the regions of low extinction ($A_V < 0.4$) at $|b| > 50°$, $I_\nu(100\,\mu m)/A_V = 18.6 MJy/sr/mag$ (Boulanger and Pérault 1988). Stars 12 and 13 (Polaris) have been added to the GF list because they are the only ones in this region having polarimetric measurements (Axon & Ellis 1976 catalogue of star linear polarization).

A few stars found to be unreddened ($E(B-V) \sim 0$) by GF could well be reddened (stars 2, 6, 8). The reddening of stars (2 and 8) but not (6) is confirmed by the E_{V-I} values. Star (7) has little reddening according to GF, and a much larger one according to Simbad. In the purely photometric work of GF any error in the reddening translates into an error in the distance. There is thus some uncertainty about the distance to star (7) which has no Hipparcos parallax. If it was reddened, its distance would have to be increased. Stars (2) and (10) indicate the presence of interstellar matter within ~ 150 pc to the Sun with $A_V \sim 0.45$ for $R_V \sim 3$. The reddening of star (8) fits with this conclusion.

Stars (5) and (6) are at a much shorter distance to the Sun, less than 100 pc. Star (5) has little but reliable reddening, with $A_V \sim 0.1$. Star (6) would have $E_{B-V} \sim 0.1$ according to Hipparcos and Simbad databases but its reddening is not confirmed by the I band which gives $E_{V-I} \sim 0$.

Stars (1), (3), (4), (9) and (11) – in italics on the table – have different spectral types in GF and Simbad. If we follow Simbad, star (1) is reddened, in agreement with the $100\,\mu$m value in this direction and the star distance (greater than 150 pc). The reddening of star (3), at 118 pc according to GF, is doubtful and less than 0.1, although the IRAS $100\,\mu$m is high in this direction. For star (4) only Simbad E(B-V) fits with the reddening of other stars at a distance larger than 150 pc. Similarly there is a large uncertainty on the reddening of star (9). GF finds more reddening than Simbad does for star (11), which can be explained by the spectral type difference between the 2 databases.

To summarize, stars at larger distances than 150 pc seem to be reddened by an amount comparable to the Polaris Flare extinction in their direction derived from the $100\,\mu$m IRAS brightness. Unfortunately data are too scarcy to be sure of any reddening at shorter distance. On the one hand, if star (3) is unreddened and GF distance reliable, a lower distance limit for the Polaris Flare is 120 pc. On the other hand, if star (6) is reddened, the Polaris Flare can be as close as 90 pc to the Sun. Star (5) reddening also indicates interstellar matter at less than 100 pc, with $A_V \sim 0.1$ mag, which could correspond to the low IRAS emission in its direction. The difficulty, therefore, still remains when attempting to reach conclusions about the reddening of stars at distances shorter than 150 pc.

Polarisation by foreground interstellar matter (Axon & Ellis 1976) has been measured for Polaris and HD 26356, only $3°$ apart. There is no polarization of HD 26356 light, which confirms the very low infrared emission at the star position. Some polarization is found in Polaris direction, which can be due either to the Polaris Flare or to some foreground interstellar cloud. These measurements do not much constrain the reddening of Polaris since its polarisation, $2\,10^{-3}$, only implies $A_V^0 > 0.08$ mag (see comparisons of stellar reddenings and polarisation in Allen's 'Astrophysical Quantities').

A.3. Conclusion

The reddening of the North star, if any is occuring, is most likely to be small because the infrared emission at the star position is low. For the surface brightness of ~ 6 MJy/sr, the expected A_V is ~ 0.3 magnitude. A similar A_V value (0.3 mag) is reported by Heithausen & Thaddeus (1990) from star counts in this region. For $R_V = 3$, a reasonable value for the low density medium in the Solar Neighboorhood, the expected reddening in Polaris direction should be close to $E_{B-V} = 0.1$ mag. The reddening of most of the stars (lines of Table A.1 which are not in italics) for which GF and Simbad spectral types are in agreement, follows the infrared emission and is of the expected magnitude. Because of uncertainties pertaining to the closest stars reddening, an upper limit for the distance to the material accounting for the IRAS emission of the Polaris Flare seems to be 150 pc to the Sun. Polaris at 133 ± 9 pc is at a critical distance. It seems it is not possible to conclude anything about its position with respect to the Polaris Flare. The linear polarimetric measurements (Axon & Ellis 1976) do indicate the presence of interstellar matter in Polaris direction. However it is not a conclusive argument because it could be accounted for by a diffuse cloud foreground to the Polaris Flare.

The complexities concerned with the question of whether Polaris is reddened or not (and if so, to what extent) are not easily derived: current data is probably not accurate enough to give both the required photometric precision and a sufficiently large sample of stars in this region. A study on a larger sample of stars distributed over the full area of the Polaris Flare, like the one done in the Chamaeleon, Musca and Coalsack region by Corradi et al. (1997), could be helpful in solving the question of the position of Polaris with respect to the Flare.

References

Arellano Ferro A., 1983a, Ph.D. Thesis, University of Toronto
Arellano Ferro A., 1983b, ApJ 274, 755
Arellano Ferro A., 1984, MNRAS 209, 481
Axon D.J., Ellis R.S., 1976, MNRAS 177, 499

Bienaymé O., Robin A.C., Crézé M., 1987, A&A 180, 94
Boulanger F., Pérault M., 1988, ApJ 330, 964
Boulanger F., Bronfman L., Dame T., Thaddeus P., 1998, A&A 332, 273
Corradi W.J.B, Franco G.A.P, Knude J., 1997, A&A 326, 1215
Cardelli J.A., Clayton, Mathis J.S., 1989, ApJ 345, 245
de Vries C.P., Le Poole R.S., 1985, A&A 145, L7
Draine B.T., Lee H.M., ApJ 1984, 285, 89
Falgarone E., Paris J.F., Heithausen A., et al., 1998, A&A 331, 669
Feltz K.A., McNamara D.H., 1980, PASP 92, 609
Fernie J.D., 1990, ApJS 72, 153
Fernie J.D., 1966, AJ 71, 732
FitzGerald M.P., 1970, A&A 4, 234
FitzGerald M.P., Stephens T.C., Witt A.N., 1976, ApJ 208, 709
Gauthier R.P., Fernie J.D., 1978, PASP 90, 739
Gordon K.D., Witt A.N., Friedmann B.C., 1998, ApJ 498, 522
Großmann V., Heithausen A., Meyerdierks H., Mebold U., 1990, A&A 240, 400
Großmann V., Heithausen A., 1992, A&A 264, 195
Guhathakurta P., Tyson J.A, 1989, ApJ 346, 773
Guhathakurta P., Cutri R.M., 1994, ASP Conf. Series 58, 34
Haywood M., Robin A.C., Crézé M., 1997, A&A 320, 428
Heithausen A., Thaddeus P., 1990, ApJ 353, L49
Helmer L., Fabricius C., Einicke O.H., Thoburn C., 1983, A&AS 53, 223
Henyey L.C., Greenstein J.L., 1941, ApJ 93, 70
Hobbs L.M., Blitz L., Magnani L., 1986, ApJ 306, L109
Johnson H.L., 1966, ARA&A 195
Kraft R.P., 1960, ApJ 131, 330
Ledoux, G., Ehbrecht M., Guillois O., et al., 1998, A&A 333, L39
Lynds B.T., 1962, ApJS 7, 1
Magnani L., de Vries C.P., 1986, A&A 168, 271
Mathis J.S., Metzger P.G, Panagia N., 1983, A&A 128, 212
Mattila K., 1971, A&A 15, 292
Meyerdierks H., Heithausen A., 1996, A&A 313, 929
Paley E.S., Low F.J., McGraw J.T., Cutri R.M., Rix H.W., 1991, ApJ 376, 335
Parsons S.B., Bouw G.D., 1971, MNRAS 152,
Robin A.C., Haywood M., Crèze M., et al., 1996, A&A 305, 125
Sandage A., 1976, AJ 81, 954
Sanwal B.B., Rautela B.S., Joshi G.C., 1988, Ap&SS 140, 131
Szomoru A., Guhathakurta P., 1999, AJ accepted
Thoraval S., Boisse P., Duvert G., 1997, A&A 319, 948
Turner D.G., 1977, PASP 89, 550
Turner D.G., Leonard P.J.T., English D.A., 1987, AJ 92, 368
Witt A.N., Stephens T.C., 1974, AJ 79, 948
Witt A.N., Schild R.E, 1985, ApJ 294, 216
Witt A.N., Gordon K.D., Furton D.G., 1998, ApJ 501, L111
Zubko V.G., Smith T.L., Witt A.N., 1999, ApJ 511, L57